CHAPTER – IV

MAGNETIZATION AND IR STUDIES

PART-A

MAGNETIZATION OF COPPER-COBALT FERRITES

INTRODUCTION

Magnetization is one of the important and fundamental parameters of the oxide magnetic materials on which various applications are based. Now a days ceramic magnets are fabricated artificially. Hence their magnetization can be altered by changing in the composition. The iron oxide based ceramic magnets viz ferrites behave in a similar way as ferromagnets. Hence parameters applicable to ferromagnetic also apply to ferrites.

The study of hysteresis provides a valuable information regarding permeability, saturation magnetization, coercivity and remanance. These parameters are very useful in deciding the particular application of ferrites. The wide range of coercivity and permeability has enabled the ferrites to have an application in the different range of frequency. Depending on porosity, anisotropy, saturation magnetization and internal stresses, the coercive force is found to vary from 10^{-1} to 10^{+3} Oe^{1}.

Besides magnetization, ferrites also exhibit the properties of switching and memory. These properties are generally affected by heat treatment, chemical composition, impurity inclusion and pressure applied during the fabrication. Morever porosity and grain size are the dominent factors in controlling the magnetic properties of ferrites[2]. Consequently the present study emphasizes the effects of such factors in determining the properties of ferrites.

The data on saturation magnetization, coercive force etc can be easily had from the hysteresis measurements. Hence this technique is used to study the magnetic parameters in the present case (Sect. 4.5).

4.1 MAGNETIC MATERIALS

The various kinds of magnetic materials are classified on the basis of susceptibility and permeability. Diamagnetic material exhibits magnetization in opposite direction of applied field. It's susceptibility is negative and permeability is less than one. Paramagnetic material possesses small positive value of susceptibility and permeability slightly greater than one. Ferromagnetic substances have the spins arranged parallel to each other as a result of strong positive interaction between the neighbouring spins.

This gives rise to large positive values of susceptibility and permeability. In antiferromagnetic materials, spins are aligned in antiparallel directions making resultant magnetization Zero, below Neel temperature. The susceptibility is not infinite at Neel temperature but has a weak cusp.

Ferrimagnetism is the term proposed by Neel[3] to describe the magnetism of ferrites. In these substances magnetic ions occupy two kinds of sublattice viz A and B. The magnitudes of spins of these lattices are opposite and unequal owing to the difference in the number and nature of atoms that make the sublattices. Such an arrangement gives rise to a resultant magnetization.

4.2 THEORIES OF FERRIMAGNETISM

In order to explain the spontaneous magnetization in ferromagnets, Weiss[4] postulated the existance of strong interactions between the neighbouring atomic dipoles to keep them parallel. Each magnetic ion is influenced by its neighbours due to internal molecular field called Weiss field. This field is proportional to the intensity of magnetization and is given by

$$H_m = \gamma M \qquad \text{- - - - - -} \quad (4.1)$$

where γ = molecular field constant

M = magnetization

In presence of external field (H), the effective field (H_e) is the vector sum of external and internal fields and is given by

$$H_e = H + H_m \qquad \text{- - - - - - - -} \quad (4.2)$$

4.2.a Neel's Theory of Ferrimagnetism

Neel putforward the concept of negative interactions between the ions on A site and B sites to promote an antiparallel alignment of moments. Besides A-B interaction, A-A and B-B interactions are taken into account though they are weak negative interactions. Then molecular field acting on an atom at A site and B site is given by

$$H_{ma} = - \gamma_{aa} M_A - \gamma_{ab} M_B$$

and $$H_{mb} = - \gamma_{bb} M_B - \gamma_{ba} M_A \qquad \text{- - - - - -} \quad (4.3)$$

where γ's are appropriate molecular field constants

M_A = Magnetization of A lattice

M_B = Magnetization of B lattice.

At equilibrium $\gamma_{ab} = \gamma_{ba}$. But in ferrimagnetics the sublattices are crystallographically inequivalent making $\gamma_{aa} \neq \gamma_{bb}$. Unless two sublattices are identical, $\gamma_{ab} > 0$

favouring antiparallel alignment of M_A and M_B giving rise to net magnetization of ferrimagnets. In presence of external field (H), total magnetic field acting on an atom in each lattice is given by

$$H_A = H - \gamma_{aa} M_A - \gamma_{ab} M_B$$

$$\text{and } H_B = H - \gamma_{bb} M_B - \gamma_{ba} M_A \qquad \text{- - - - -} \quad (4.4)$$

(i) Paramagnetic Region

In an assembly of N atoms per unit volume, each with angular momentum quantum number J, the sublattice magnetizations are represented by

$$M_A = \frac{C_a}{T} H_{ma} \quad \text{and} \quad M_B = \frac{C_b}{T} H_{mb} \qquad \text{- - - - -} \quad (4.5)$$

$$\text{where } C_a = \sum_i N_i g^2 \mu_B^2 S_i (S_i+1)$$

$$C_b = \sum_j N_j g^2 \mu_B^2 S_j (S_j+1)$$

here N_i and N_j are number of atoms/unit volume with spin quantum numbers S_i and S_j respectively.

g = Lande's factor

μ_B = Bohr magneton.

Now the volume susceptibility can be defined as

$$\chi = \frac{M_A + M_B}{H} \qquad \text{- - - - -} \quad (4.6)$$

By substituting the values of M_A and M_B from equation (4.5) in equation (4.6) and simplifying further the expression for inverse susceptibility becomes

$$\frac{1}{\chi} = \frac{T}{C} + \frac{1}{\chi_o} - \frac{\sigma}{T - \theta} \qquad \text{---- (4.7)}$$

where $C = C_a + C_b$

$$\frac{1}{\chi_o} = \frac{1}{C^2} \left(C_a^2 \gamma_{aa} + C_b^2 \gamma_{bb} + 2 C_a C_b \gamma_{ab} \right)$$

$$\sigma = \frac{C_a C_b}{C^3} \left\{ \begin{array}{l} C_a^2 (\gamma_{aa} - \gamma_{bb})^2 + C_b^2 (\gamma_{bb} - \gamma_{ab})^2 \\ -2C_a C_b \left[\gamma_{ab}^2 - (\gamma_{aa} + \gamma_{bb}) \gamma_{ab} + \gamma_{aa} \gamma_{bb} \right] \end{array} \right\}$$

$$\theta = - \frac{C_a C_b}{C} \left(\gamma_{aa} + \gamma_{bb} - 2N \gamma_{ab} \right)$$

Equation (4.7) represents the hyperbola which cuts the temperature axis at $\theta = - \frac{C}{\chi_o}$ (Fig.4.1)

where 'θ' is asymptotic Curie point. The asymptote is given by (as $T \rightarrow \infty$)

$$\frac{1}{\chi} = \frac{T}{C} + \frac{1}{\chi_o} \qquad \text{----- (4.8)}$$

$\therefore$ the expression for volume susceptibility becomes

$$\chi = \frac{C}{T + \theta} \qquad \text{----- (4.9)}$$

where $\theta > 0$

The quantity $\frac{1}{\chi}$ becomes Zero at 'θ', where X becomes

theoretically infinity or X is practically very large and the substance passes from the paramagnetic to ferrimagnetic with decrease in temperature. In otherwords the substance obeys Curie-Weiss Law with asymptotic Curie point 'θ'.

(ii) Spontaneous Magnetization

At low temperature the magnetizations of the sublattices of ferrimagnetic substance form the spontaneously magnetised systems. The expressions for spontaneous magnetizations are given by

$$M_{Asp} = N_a g \mu_B S_a B_a X_a$$

$$\text{and } M_{Bsp} = N_b g \mu_B S_b B_b X_b \qquad \text{- - - - -} \quad (4.10)$$

where B's are Brillouins functions

N's are number of atoms per unit volume of appropriate lattices

S's are spin quantum numbers of atoms at appropriate lattices

$$X_a = \frac{S_a \mu_B g}{KT} \left(\gamma_{ab} M_B - \gamma_{aa} M_A \right)$$

$$X_b = \frac{S_b \mu_B g}{KT} \left(\gamma_{ab} M_A - \gamma_{bb} M_B \right)$$

$\therefore$ the net spontaneous magnetization can be written as

$$M = \left| M_{Bsp} - M_{Asp} \right| \qquad \text{- - - - -} \quad (4.11)$$

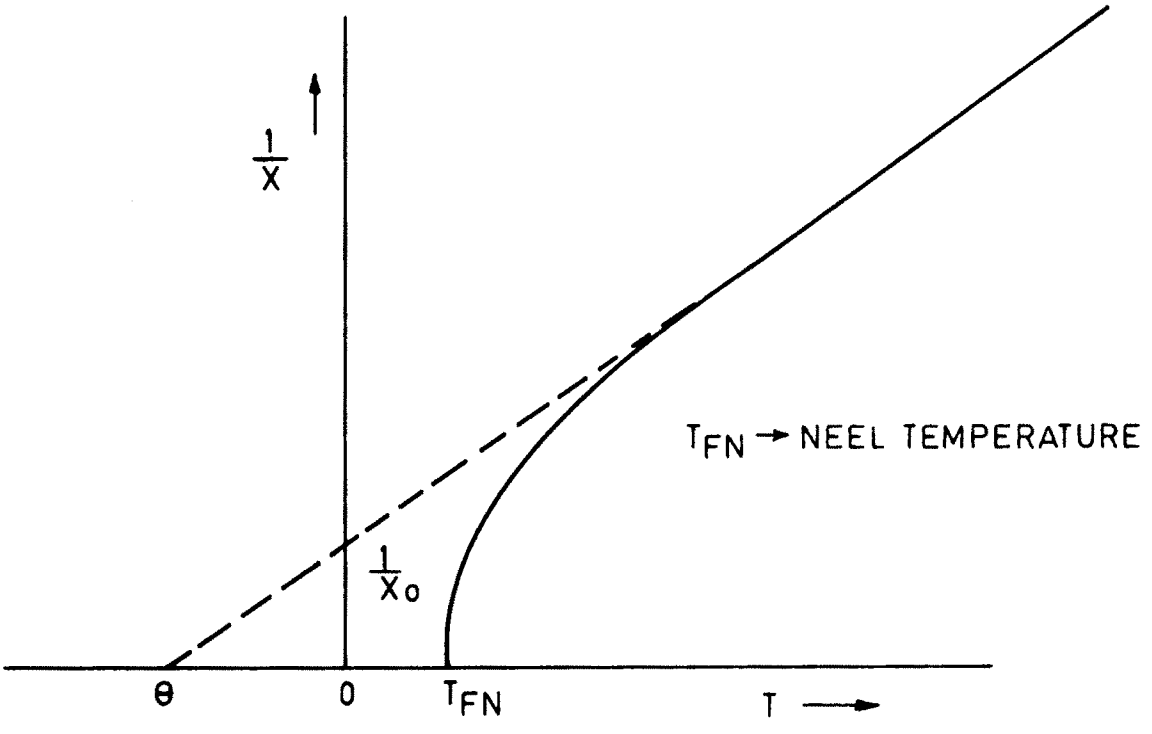

FIG. 4·1 INVERSE SUSCEPTIBILITY($\frac{1}{X}$) VS TEMPERATURE (T).

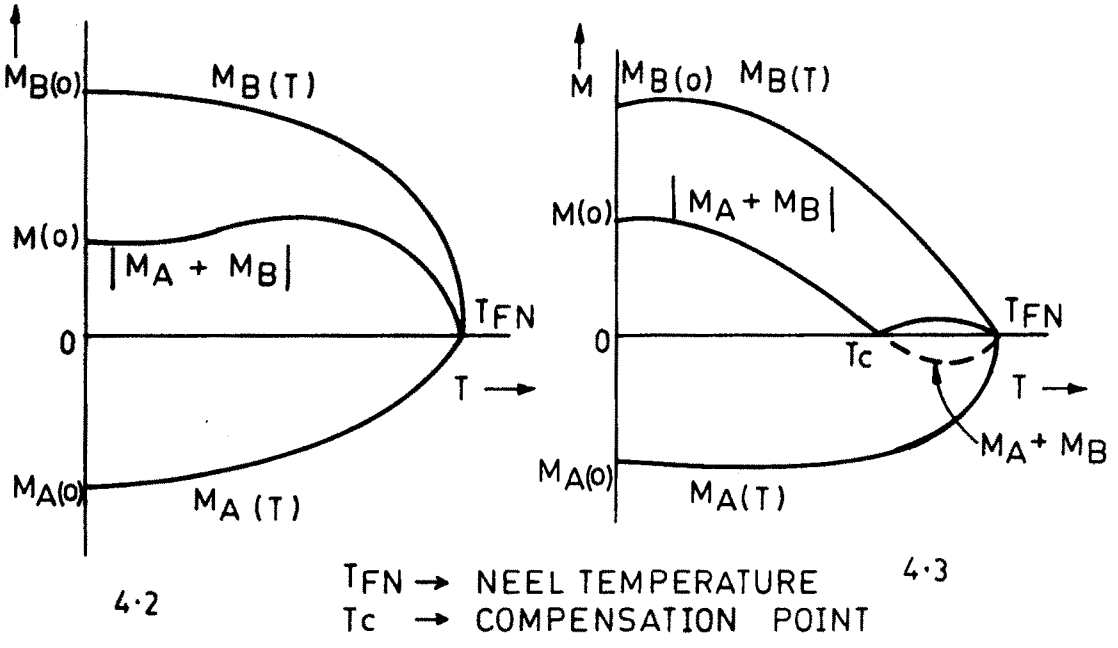

FIG. 4·0 SPONTANEOUS MAGNETIZATION (M) VS TEMPERATURE (T).

The graphs of M versus T are shown in Fig 4.2 and 4.3. Such curves are of different variety. They provide information about spontaneous magnetization and exchange energy at different temperature. The above theory is supported by experimental curves of Neel[3], Gorter[5] and Smart[6].

4.2.b Yafet-Kittel Theory

Neel's theory stands good for pure ferrites. But it is inadequate for the spinels which contain other than iron ions. Therefore Yafet and Kittel[7] proposed triangular type of spin arrangements.

They considered the possibility of subdivision of each lattice to account for the magnetic ordering within the lattice, other than parallel arrangement of spins. They found that when strong negative interaction exists within the sublattice B, the two equivalent sublattices B_1 and B_2, being spontaneously magnetised, are not exactly antiparallel. Instead they align at some angle other than 180°. Thus there is a resultant magnetization of B lattice setting antiparallel to the magnetization of A lattice.

These triangular arrangements within the lattice result in values of reduced magnetization of the same order

and magnitude as those predicted by Neel model. However they are free from thermodynamic difficulties near absolute Zero. The interaction energy for this case is given by

$$E = 8N \left[6J_{ab} S_a S_b \cos\phi - J_{bb} S_b^2 (2\cos\phi - 1) \right] \qquad \text{- - - - - (4.12)}$$

where ϕ = Angle between A and subdivisions of B

$J's$ = Exchange integrals.

Interaction energy is minimum for J_{ab} negative and J_{bb} positive. If $\phi = 0$, then Neel's state is obtained. If J_{bb} is also negative, then the ratio of exchange energies is given by

$$\gamma_{ex} = \frac{J_{bb} S_b}{J_{ab} S_a} > \frac{3}{4} \qquad \text{- - - - - (4.13)}$$

Under such condition Neel's state will not be minimum and magnetization of sublattice B_1 and B_2 will be inclined to sublattice A at an angle given by

$$\cos\phi = \frac{3}{4} \frac{J_{ab} S_a}{J_{bb} S_b} \qquad \text{- - - - - (4.14)}$$

They proved that Neel's structure is stable for $\gamma_{ex} < \frac{3}{4}$, if the total number of sublattices is restricted to six. The existance of triangular arrangement has been reported by Lotering[8] in some particular cases.

4.2.c Spiral Spins

Lyons and Kaplan[9] have given a generalised treatment of spin configuration along with Y-K model. They have suggested the possibility of spiral or helical spin arrangements by neutron diffraction in some compounds and showed that they have lower energy for all values of $\gamma_{ex} > \frac{2}{3}$. Corliss and Hastings[10] observed the existance of such configuration in manganese chromite. Similarly spiral spin configuration has been reported by EnZ[11] in hexagonal ferrites.

4.3 MAGNETIZATION IN FERRITES

The exchange interaction between the magnetic moments of neighbouring atoms is responsible for the magnetization in ferrites. The interaction is said to be positive when the moments are parallel and negative when the moments are antiparalle. However for incomplete 'd' shell the exchange interaction may be either positive or negative. Therefore the intrinsic magnetization in ferrites can be attributed to the antiparallel arrangements of spins of sublattices, assuming inverse spinel type ion distribution.

Generally ferrites have mixed structure with fraction

of trivalent ions on A sites and remainder on B sites. The parallel arrangement results either in antiferromagnetism or ferrimagnetism depending on whether the moments cancel completely or partially.

The spinning electrons are exchanged between the neighbouring atoms, giving rise to exchange force and exchange energy. The exchange energy forms an important part of the total energy in certain compounds such as spinel ferrites. The interaction energy of atoms i and j with spins S_i and S_j is represented by the equation

$$E_{ex} = -2 S_i S_j J_{ex}$$

$$= -2 S_i S_j J_{ex} \cos \phi \qquad ------ \quad (4.15)$$

where J_{ex} = Exchange integral

ϕ = Angle between spin vectors of S_i and S_j

$\therefore$ Total exchange energy is obtained by taking summation over equation (4.15)

$$\therefore W_{ex} = -2 S^2 J \sum_{i \neq j} \cos \phi_{ij} \qquad ------ \quad (4.16)$$

where S = Total spin momentum

J = Total exchange integral.

When the exchange integral is positive, parallel alignment of spins is favoured resulting in ferromagnetism.

In general exchange integral is negative resulting in antiparallel spin arrangements giving rise to antiferromagnetism. Such an ordered arrangement of spins causes for the resultant spontaneous magnetization in ferrites, in absence of any external magnetic field.

The temperature at which the long range order sets in (Neel temperature) is determined largely by the strength of interaction between neighbouring ions. In case of both ferromagnetic and antiferromagnetics, the interaction arises from an indirect exchange mechanism in which magnetic ions are coupled through electron transfer with intermediate anions. This concept of indirect exchange was putforward by Kramers[12] and then developed by Anderson[13] in the form of super exchange. The idea of super exchange is used to explain magnetization in normal and inverse spinels.

4.4. MAGNETIC HYSTERESIS

When a ferromagnetic substance is subjected to an external field, its magnetization increases as a function of applied field and reaches saturation value at certain critical field. On decreasing the external field demagnetization is not recovered completely. Thus

magnetization appears to lag behind the applied field. Such behaviour is called the phenomenon of hysteresis. In order to explain this phenomenon Weiss postulated the existance of magnetic domains.

The variation of saturation magnetization with applied field is shown in Fig (4.4). As the applied field increases magnetization goes on increasing continuously till it reaches a saturation value at a certain value of field. This behaviour is represented by the curve OABC and is called magnetization curve. The variation of magnetization of specimen per cycle of magnetization is represented by the curve CDEFGC and is called hysteresis loop. The loss of energy due to hysteresis is equal to the area of the loop.

The slope of the tangent to the magnetization curve at the origin (ox) gives the magnitude of initial susceptibility (Xo). It plays an important role in magnetic recording as it decides the distortion factor. Maximum susceptibility occurs near knee of the magnetization curve (slope-oy).

The magnitude of magnetization for Zero field (H = 0)

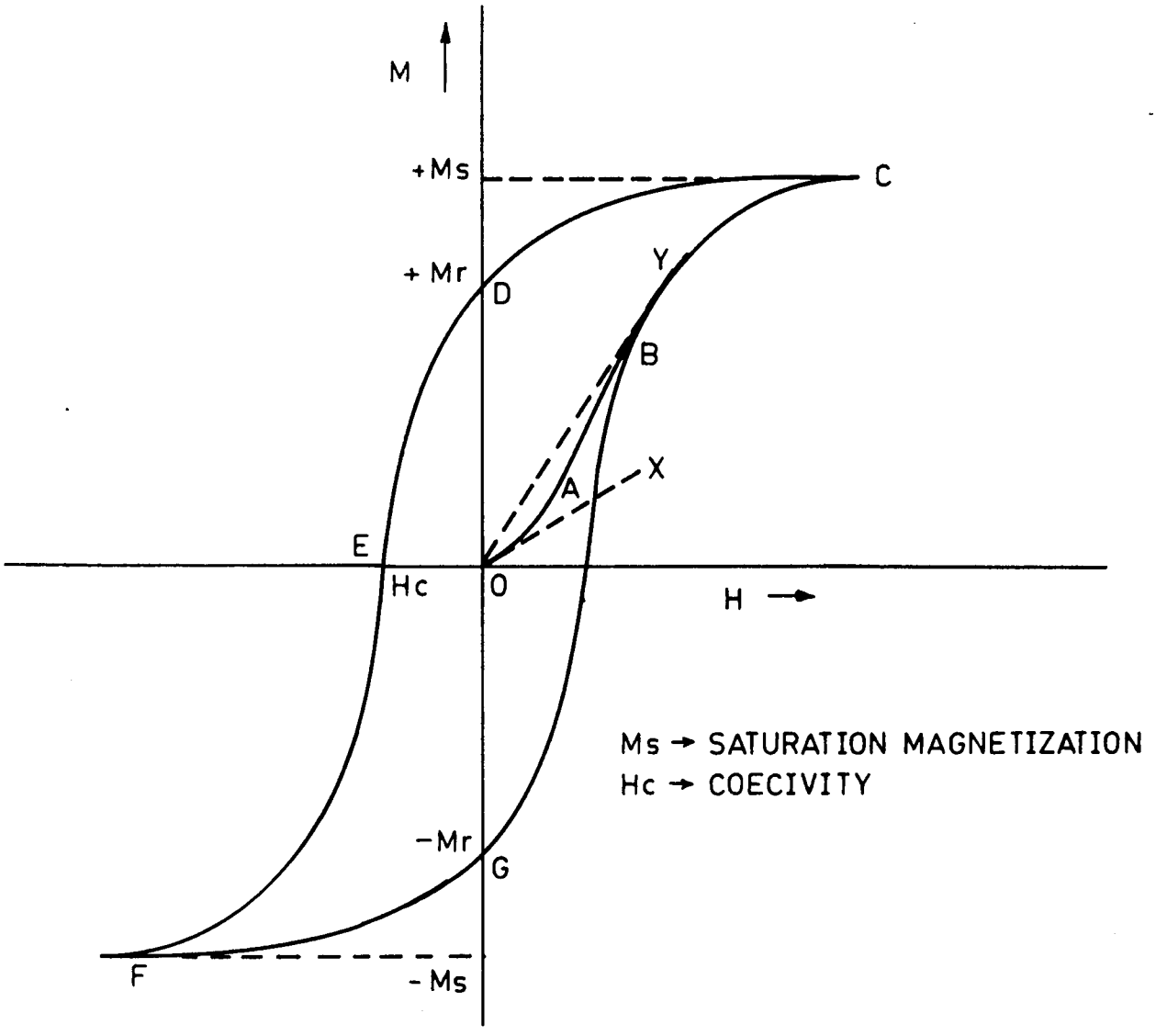

FIG.4·4 MAGNETIZATION CURVE (OABC) AND HYSTERESIS LOOP (CDEFGC)

is retentivity or remanance (M_r). The value of reverse field for which magnetization is Zero (M=0) is called coercive force (H_c). The magnetization corresponding to point 'C' is saturation magnetization (M_s). The coercivity and retentivity are the important parameters in selecting the material for permanent magnet applications.

4.5. EXPERIMENTAL TECHNIQUE

The saturation magnetization is measured using high field loop tracer, assembled by Tata Institute of Fundamental Research, Bombay.

The loop tracer consists of an electromagnet capable of working on 50 Hzs mains supply. The sinusoidal magnetic field of about 3600 oe is produced in an air gap of about few mm in the instrument and a special balancing coil is used to measure the saturation magnetization of the sample in the air gap. The actual experimental set up is shown in the photograph of Fig (4.5). The signal proportional to the magnetic moment of the sample is supplied to the vertical plates of oscilloscope with requisite amplification, while the signal proportional to the applied field is fed to the horizontal plates of oscilloscope. The vertical

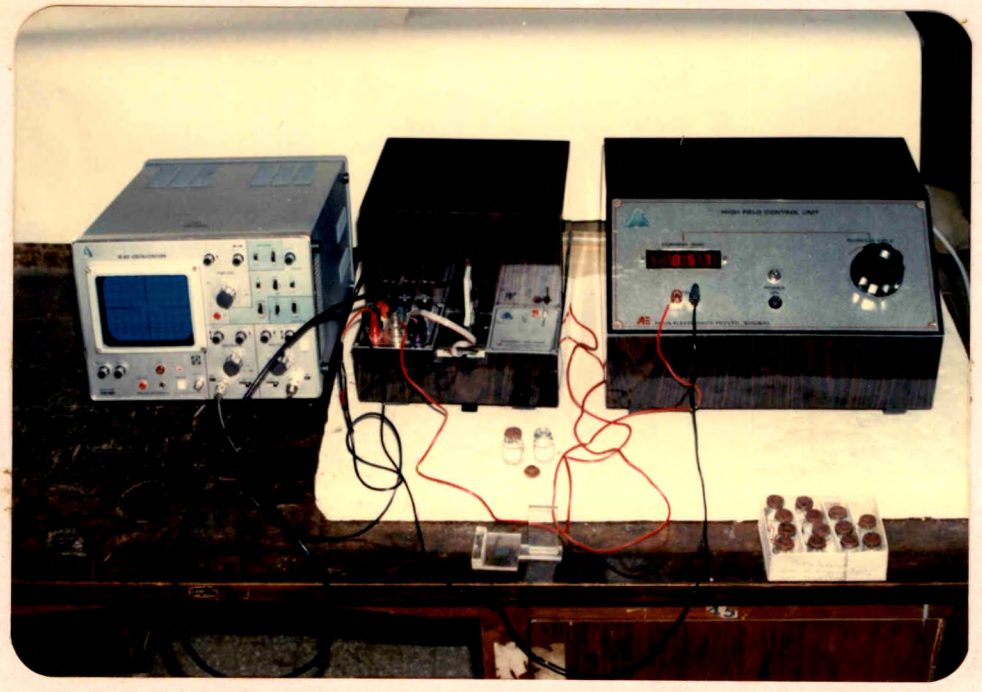

Fig. 4·5 EXPERIMENTAL SET UP FOR HYSTERESIS LOOP MEASUREMENT

displacement of hysteresis loop on the oscilloscope is measured with the help of digital multimeter in milli volts (mv).

The apparatus, in general, consists of

(i) C-core unit to feed the sample and to amplify the signal in C-core

(ii) Control unit to supply the power

(iii) Display unit to exhibit the hysteresis loop on CRO and to carry out quantitative measurement with the help of digital multimeter.

To start with, the high voltage cable is connected from control unit to C-core unit. Balancing coil is mounted on 12 pin connector associated with C-core unit and introduced into air gap in an instrument. The vertical and horizontal outputs of C-core unit are fed to the vertical and horizontal inputs of the control unit respectively. The vertical output of control unit is connected to the vertical input of the oscilloscope and horizontal output to EXT horizontal. Keeping vertical gain control at low positive, current is increased upto 300 ma with the help of control unit to get an ellipse on the screen. To convert the ellipse into the straightline, the vertical phase control is adjusted. The

straightline is rotated to make the phase difference Zero by changing the 'coarse' amplitude potentiometer. After this setting, the balancing coil is taken out of the C-core gap.

The vertical displacement on CRO is calibrated by loading pure nickel sphere of mass 1.913 grams between the pole pieces. This gives the vertical displacement of 1010 mv after eliminating background noise voltage. As the standard magnetization for nickel is 53.34 emu/gram, total magnetization of nickel sphere is 53.34 x 1.913 = 102 emu.

$\therefore$ Calibration factor = $\frac{102}{1010}$ = 0.10099 emu/mv.

The vertical displacements for each sample are noted by introducing each pellet separately into the air gap between the pole pieces and are tabulated in table 4.1 along with sintering temperature and time. The saturation magnetization is calculated by the relation

σ_s = V x calibration factor -- - emu - - -- (4.17)

where V = Vertical displacement for a given sample on CRO

$\therefore$ Saturation magnetization in emu/gr is given by

$$\sigma_s' = \frac{\sigma_s}{\text{mass of sample}} \text{ - - - emu/gr - - - - (4.18)}$$

TABLE 4.1

VERTICAL DISPLACEMENTS FOR $Cu_x Co_{1-x} Fe_2O_4$ IN CRO

Sample	Sintering temperature (^oC)	Sintering time (hrs)	Vertical displacement (mv)
$CoFe_2O_4$	800	20	850
"	900	20	862
"	900	30	905
$Cu_{0.4}Co_{0.6}Fe_2O_4$	800	14	136
"	900	20	161
"	900	30	170
$CuFe_2O_4$	800	20	270
"	900	20	326
"	900	30	341

Similarly saturation magnetization in emu/cc for a given porosity is calculated by the relation

$$M_s = (1-P)\, d_x . \overline{\sigma_s} \quad \text{- - - - emu/cc - - - - (4.19)}$$

where P = Porosity = $\frac{d_x - d_a}{d_x}$

d_x = X-ray density

d_a = Actual density

and saturation magnetization in gauss is calculated by $4\pi M_s$. The magnetic moment per molecular formula unit in Bohr magnetons is calculated by

$$M_B = \frac{\text{Molecular weight} \times \overline{\sigma_s}}{5585} \text{ -- - Bohr magnetons} \quad \text{- - - - (4.20)}$$

4.6. RESULTS AND DISCUSSION

The calculated values of magnetization and magnetic moment are tabulated in table 4.2. The table indicates the variation of saturation magnetization with firing temperature and time. The samples fired at 900°C for longer time show greater magnetization values than the others. This behaviour can be explained on the basis of redistribution of cations[14] with sintering temperature and time and also on the basis of microstructural changes brought in by firing conditions. The effect of structural variation and

TABLE 4.2

MAGNETIZATION OF $Cu_x Co_{1-x} Fe_2O_4$ FERRITES

Sample	Sintering temp/time (^oC, hr)	Porosity P	Saturation Magnetization		Magnetic moment M_B Bohr Magneton
			M_s emu/cc	$4\pi M_s$ Gauss	
$CoFe_2O_4$	800, 20	0.3219	308	3871	3.714
"	900, 20	0.2399	350	4399	3.955
"	900, 30	0.2016	386	4852	4.041
$CuFe_2O_4$	800, 20	0.2951	111	1395	1.306
"	900, 20	0.2341	142.4	1781	1.533
"	900, 30	0.1904	157.6	1980	1.482
$Cu_{0.4}Co_{0.6}Fe_2O_4$	800, 14	0.3347	48.9	616	0.7042
"	900, 20	0.3105	60	753.6	0.9984
"	900, 20	0.2916	65	818.6	0.8884

distribution of cations over octahedral and tetrahedral sites on magnetization has been discussed in case of Co-Zn ferrite[15] to obtain the correlation between microstructure and magnetic properties. The reduced porosity at higher sintering temperature has a considerable effect on magnetization of all the samples studied here. This is in accordance with results reported earlier[16].

In general, all spinel ferrites are more or less inverse. It means some of the divalent metal ions prefer octahedral B sites and equal fraction of trivalent iron ions prefer tetrahedral A sites. The degree of inversion depends upon the heat treatment. The increase in temperature causes the excitation of the ions of sublattices and consequently changes the structure from normal to inverse. The resultant magnetization is the vector sum of sublattice magnetizations.

Prince[17] had reported complete inverse spinel structure in $CoFe_2O_4$ by neutron diffraction. If this is the case the theoretical magnetic moment would be 3 Bohr magneton. However in the present case it is observed to vary between 3.714 to 4.041 Bohr magneton (Table 4.2). The higher values than theoretical can be ascribed to the contribution of orbital moment to spin moment and to extent of inversion.

Sawatzky and others[18] have reported partial inverse spinel structure in $CoFe_2O_4$. Hence in the present case partial inverse spinel structure is assigned to the cobalt ferrite and accordingly the cation distribution is given by

$$Fe^{3+}_{1-\delta} \quad Co^{2+}_{\delta} \quad (Co^{2}_{1-\delta} \; Fe^{3}_{1+\delta}) \; O^{2-}_{4}$$

where δ = coefficient of normalcy less than one

The spin moments for Fe^{3+}, Co^{2+} and Cu^{2+} are 5, 3 and 1 Bohr magnetons respectively. The resultant magnetic moment per formula unit is given by

$$\mu_B = 3 + 4\delta \qquad \text{- - - - -} \quad (4.21)$$

The experimental values of μ_B for cobalt ferrite are 3.714, 3.955 and 4.041 respectively (Table 4.2). From the equation 4.21, δ comes out to be 0.1785, 0.24 and 0.26. It can be concluded that the normalcy in cobalt ferrite varies from 15% to 30%, depending on preparation condition. The calculated saturation magnetization values agree well with the values reported earlier[19]. However the variation is assumed to be due to the method of preparation.

The partial inverse spinel structure in copper ferrite has been reported on the basis of variation of experimental results from theoretical values of magnetic moment[20,21]. In the present case magnetic moment of copper ferrite varies

from 1.306 to 1.533 Bohr magnetons (Table 4.2), whereas its theoretical value is 1 Bohr magneton for complete inverse structure. Therefore the copper ferrite under study is proposed to have a partial inverse spinel structure and accordingly the cation distribution is given by

$$Fe^{3+}_{1-\delta}\ Cu^{2+}_{\delta}\quad (\ Cu^{2+}_{1-\delta}\ Fe^{3+}_{1+\delta}\ )\ O^{2-}_{4}$$

where δ = coefficient of normalcy less than one

The magnetic moment per formula unit is represented by

$$\mu_B = 1 + 8\delta \qquad \text{- - - - -} \quad (4.22)$$

substituting the experimental values of μ_B from table 4.2, it is found that δ varies between 0.0375 to 0.06662 depending on preparation condition. Hence it can be inferred that the degree of inversion in copper ferrite varies from 93 to 97%, depending on heat treatment. The calculated values of saturation magnetization are comparable to the reported values[19]. The deviations are attributed to the preparation techniques.

The addition of copper to cobalt ferrite causes the copper ions to occupy A sites replacing some of the Fe^{3+} ions, which in turn occupy B sites by vacating Co^{2+} ions. This causes the decrease in the magnetization of A sites as copper percentage increases. At x = 0.4, the cation

distribution for the sample $Cu_{0.4}\ Co_{0.6}\ Fe_2O_4$ can be represented as

$$Cu^{2+}_{0.4}\ Co^{2+}_{0.4}\ Fe^{3+}_{\delta}\ \left(\ Co^{2+}_{0.2}\ Fe^{3+}_{2-\delta}\ \right)\ O^{2-}_{4}$$

the calculated values of δ vary between 97 to 99.8%, depending on heat treatment. This shows that A and B sites are almost equally occupied by Fe^{3+} ions. Hence resultant magnetization is mainly due to the ions at A sites which contribute small amount to magnetization. Therefore the observed magnetization of this sample is comparatively small.

From the table 4.2 it is evident that magnetization changes with heat treatment. As temperature increases ions diffuse from B sites to A sites and vice-versa. This causes the ferrites to have partial inverse spinel structure. Magnetization studies can be utilised to determine their cation distribution.

Another important factor that influences the magnetization of ferrites is their microstructure. Each grain has certain amount of resultant magnetic moment. The presence of pores breaks the magnetic circuits among the grains, resulting in net reduction of magnetization, with

increased pore concentration. On the other hand grain boundary opposes the motion of domain walls. Under large concentration of pores the total area of grain boundary increases offering a high resistance to domain wall motion, in turn to magnetization. For a sample sintered at higher temperature and time, net area of grain boundary decreases due to densification and low porosity. As a result the domain walls become more mobile to increase the magnetization. This implies that when crystallites become large with negligible porosity, crystalline anisotropy decreases making magnetization easy. Such a behaviour can be observed in electron micrographs of our samples (Fig.5.1 to 5.6). Thus the texture of grains is important in ferrites where the magnetization has strong preference for a particular crystallographic direction (called easy axis of magnetization) or magnetic anisotropy.

Polycrystalline materials with large number of grains have domain structure similar to single grain materials. But domain structure is modified due to interaction between the neighbouring grains in fine grained materials[22]. Lower sintering temperature causes large number of small grains. Whereas higher sintering temperature gives small number of

large grains and consequently reduced porosity. The linear relationship has been reported between permeability and grain diameter[23,24]. In the present case electron micrographs show greater grain diameter at higher sintering temperature. The rise magnetization value is in accordance with rise grain diameter in the present case.

There is also a possibility of formation of closed pore chains at low firing temperature, leading to the decrease in magnetization. Such an idea has been supported by Rikukawa[25] proposing the diamagnetic field caused by closed pores and boundries. Hence magnetization decreases at low sintering temperatures. The electron micrographs are the convincing evidence for the occurance of such phenomenon.

PART-B

FAR INFRARED SPECTRA OF $Cu_xCo_{1-x}Fe_2O_4$ FERRITES

INTRODUCTION

Electromagnetic radiation in which wavelengths lie in the range of 1 μto 1 mm is termed as infrared radiation. It has a wavelength just little longer than those of visible light.

The optical spectra of ferrites give information about the various vibrational modes in the presence or absence of Fe^{2+} ions in the ferrites whereas the vibrational electronic and magnetic dipole spectra provide information about the position and valency of the ions in the crystal lattice. Infrared spectra are used to detect the presence of absorption or emission bands in the ferrites. It has become the powerful tool in the hands of analytical chemists and physicists, since it provides unmistakable " finger prints ".

According to group theoretical considerations, Waldron[26] reported four optical bands corresponding to four infrared active fundamentals (T_1u) in the vibrational spectra of normal as well as inverse cubic spinels. Out of four bands two corresponding to high frequencies, are broad and

assymetric, depending upon the preparation condition and grain size. They may give rise to distinct shoulder or even splitting of bands. The other two bands corresponding to low frequencies are quite sharp and unaffected by the preparation condition.

Generally four active infrared bands are reported in the range of 100 cm^{-1} to 1000 cm^{-1}. Waldron[26] observed two bands in different ferrites in the region of 200 cm^{-1} to 1000 cm^{-1}. He attributed the high frequency band γ_1 to tetrahedral complexes and low frequency band γ_2 to octahedral complexes. Also he noticed the gradual increase in the absorption of higher frequencies caused by electronic transition.

Hafner[27], Tarte[28] and others[29,30] applied infrared spectroscopy to investigate the absorption bands in many normal as well as inverse spinel ferrites. Brabers[31] observed the splitting of bands in cubic and tetragonal manganese ferrites $Mn_xFe_{3-x}O_4$ in the range of 700 cm^{-1} with $x > 1$ and concluded that there are local tetragonal distortions originating from the Jahn-Teller effect of the octahedral Mn^{3+} ions.

Infrared spectra of $MnFe_2O_4$ with inversion degree of Mn

about 0.05 and 0.2 was studied by Klerk[32]. He concluded that the absorption observed at 335 cm^{-1} has to be third fundamental IR active mode. In addition to IR studies properties like anisotropy, structure of domains etc were also studied by several workers[33,34,35].

4.7 EXPERIMENTAL TECHNIQUE

The far infrared spectra of cobalt, copper-cobalt and copper ferrite were obtained from Indian Institute of Science, Bangalore (India), using the Beckman Infrared Spectrophotometer. In order to cover the wide range of frequency available with the instrument, beam devices of different thicknesses were employed. The spectrum was taken in the range of 50 to 700 cm^{-1}. As no bands were observed in the range 50 to 200 cm^{-1}, the range of spectrum was taken from 200 to 700 cm^{-1}. The interferrometer chamber was kept under vacuum to avoid the effect of moisture of water vapour which would affect the spectrum in this region.

4.8 RESULTS AND DISCUSSION

The spinel ferrites crystallise into cubic form with space group $Fd3_m$-O_h^7. On the basis of space group and point symmetry, group theoretical calculations show four IR active

fundamentals (T_1u) in the vibrational spectra of normal and inverse cubic spinel structure. The vibrational frequencies depend upon cation mass, cation-oxygen bonding force and distance and parameter of the unit cell.

The IR of cobalt, copper-cobalt and copper ferrite are shown in Fig. 4.6, 4.7 and 4.8 respectively. The spectra of these ferrites were used to locate the position of absorption band and band positions are shown in Table 4.3.

In the present study, the absorption bands are found to be in the same expected frequency range. The higher frequency band γ_1 is in the range of 550 to 575 cm^{-1}, while the lower frequency band γ_2 is in the range of 400 to 470 cm^{-1}. From the Table 4.3 it is seen that there is a little change in the band positions of the spectra. The main cause for such changes is the difference in the Fe^{3+}- O^2 band distance for B and A sites.

Waldron[26] and Hafner[27] were the pioneers to study the vibrational spectra of ferrites. They attributed the band around 600 cm^{-1} to the intrinsic vibrations of the tetrahedral complexes and that around 400 cm^{-1} to the vibrations of octahedral complexes. However Tarte and Preudhomme[36] reported that both the observed absorption bands in spinel ferrites

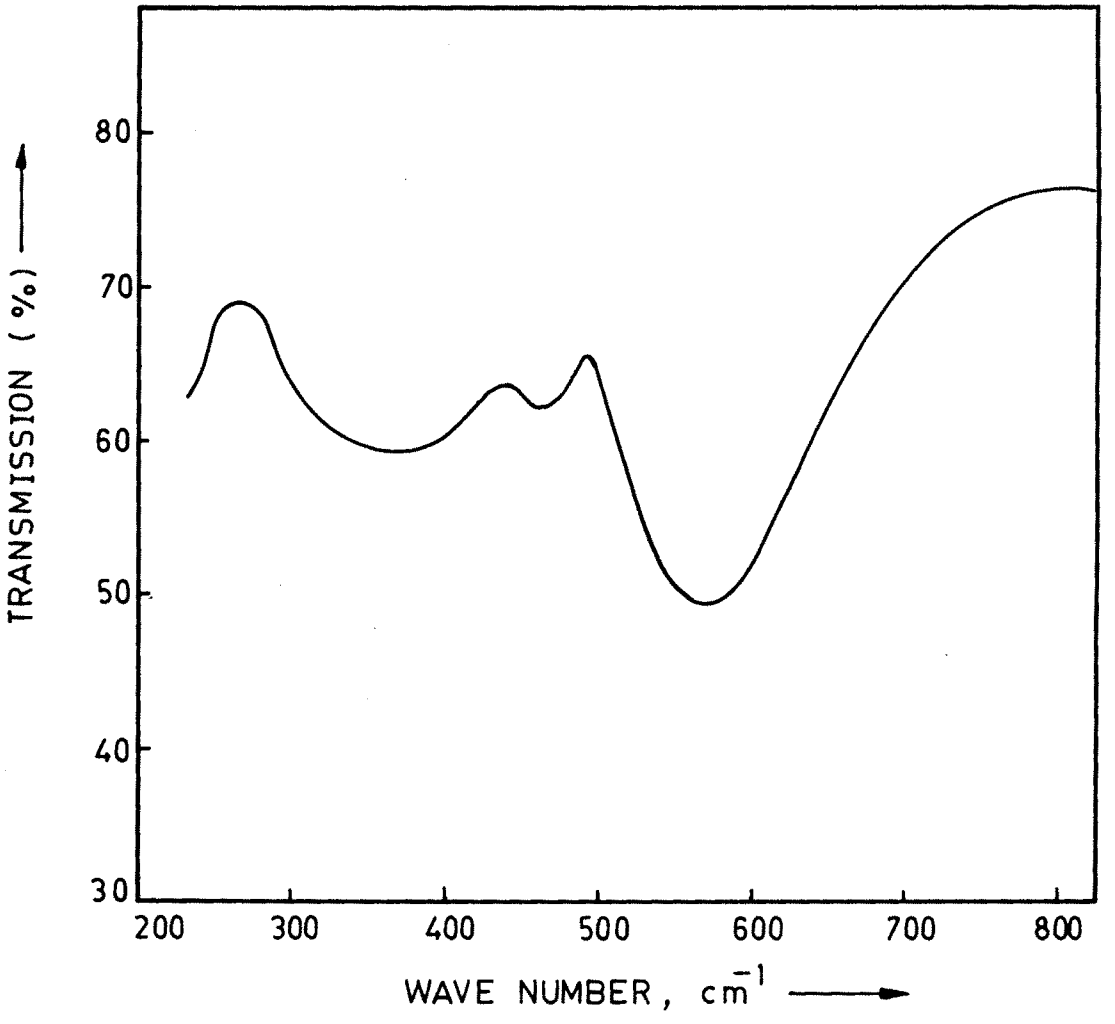

Fig. 4·6 THE FAR INFRARED SPECTRUM OF $CoFe_2O_4$.

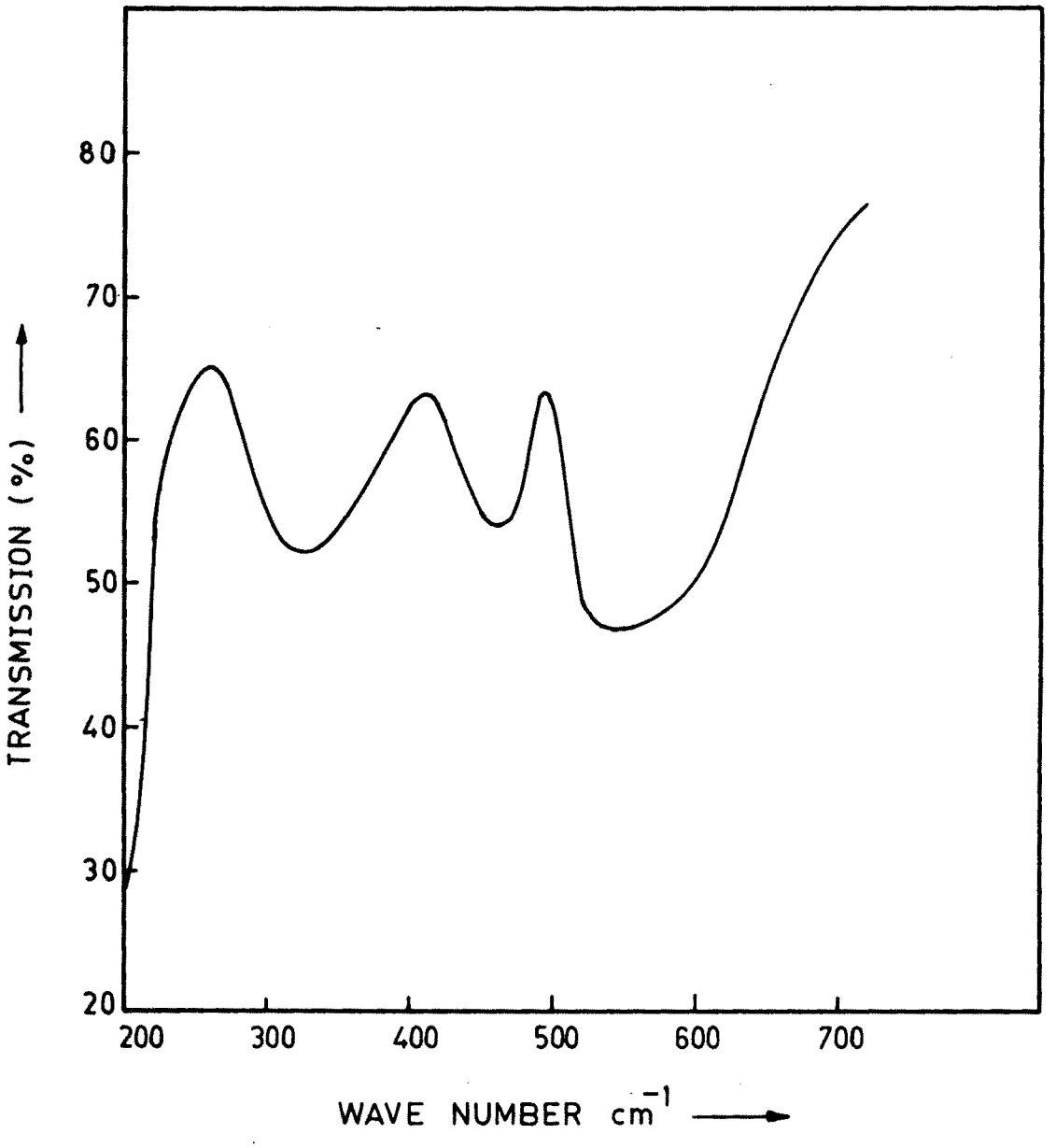

Fig. 4·7 THE FAR INFRARED SPECTRUM OF $Cu_{0.4}Co_{0.6}Fe_2O_4$

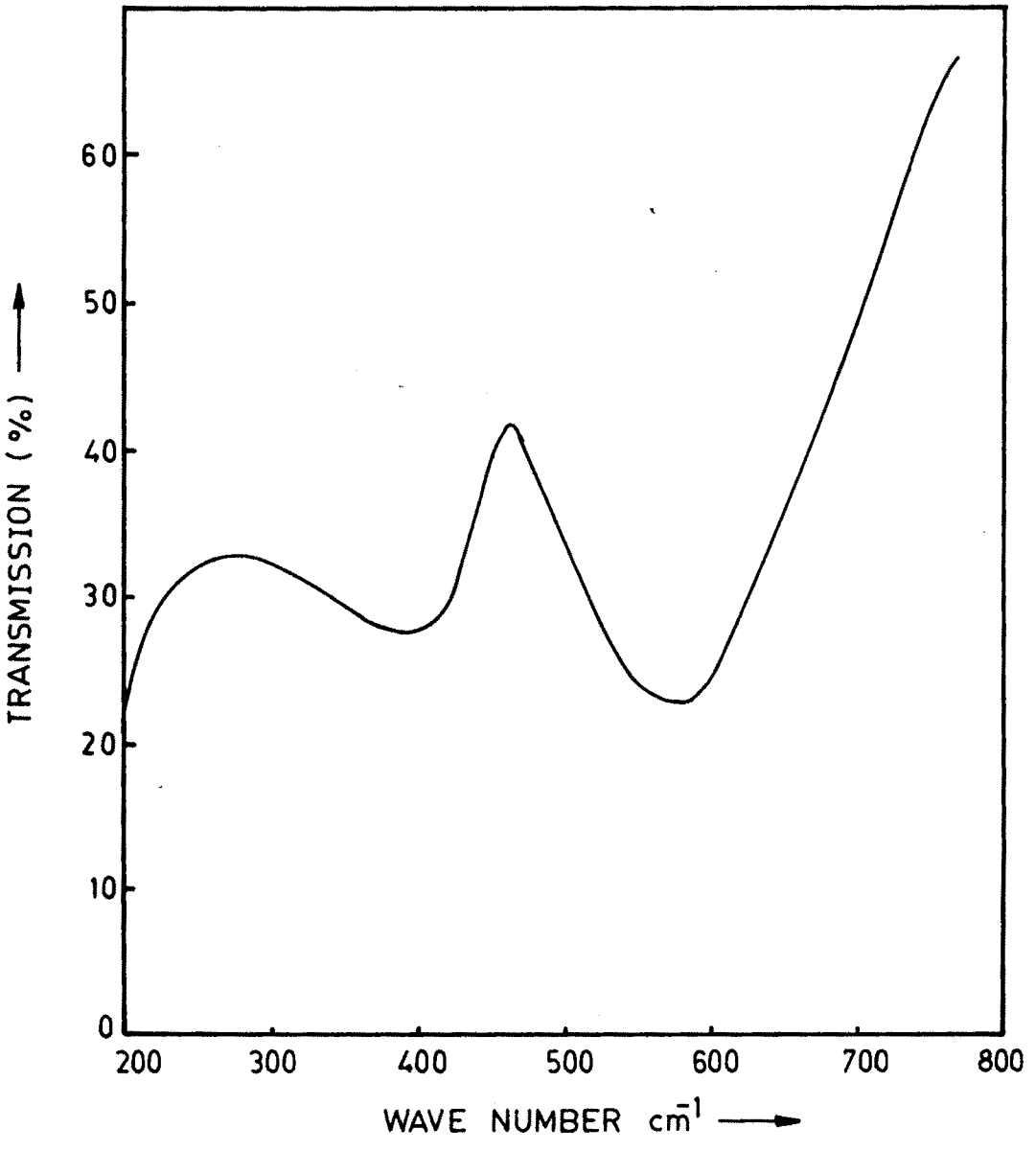

Fig. 4·8 THE FAR INFRARED SPECTRUM OF $CuFe_2O_4$.

depend on the nature of octahedral cation significantly but not on the nature of tetrahedral ions. Botakova et al[37] studied the IR of Ni-Zn mixed ferrites and concluded that Fe^{2+} ions are occupying both A and B sites.

An examination of the Table 4.3 and IR spectra (Fig. 4.6 to 4.8) reveals that a small band γ_3 around 400 cm^{-1} appears for certain concentrations of cobalt (0.6, 1.0) in copper ferrite. For the lowest concentration (x =1) this band is not visible. However the broadness and shape of the spectrum (Fig.4.8) suggests the possibility of such band. As cobalt concentration increases the intensity of the band γ_3 increases and reaches maximum at x =0. This causes the band γ_2 to become more narrow.

From the Table 4.3, also it is seen that the bands γ_1 and γ_2 vary slightly from ferrite to ferrite. This change is the consequence of the change in $Fe^{3+} - O^{2-}$ bonding distance with the increase of cobalt concentration. As the band γ_2 is attributed to octahedral complexes, the appearance of γ_3 around γ_2 may be due to octahedral origin. The increase of cobalt concentration increases the strength of $Co^{2+} - O^{2-}$ bonding and hence increase in the intensity of γ_3 band is expected. This is strongly supported by the present results

TABLE 4.3

FAR INFRARED SPECTRA DATA OF $Cu_xCo_{1-x}Fe_2O_4$ FERRITES

Sample	Frequency of absorption bands			
	$\gamma_1 cm^{-1}$	$\gamma_2 cm^{-1}$	$\gamma_3 cm^{-1}$	$\gamma_4 cm^{-1}$
$CoFe_2O_4$	570	470	370	-
$Cu_{0.4}Co_{0.6}Fe_2O_4$	550	460	330	-
$CuFe_2O_4$	575	400	-	-
$NiFe_2O_4$*	587	396	-	-
$MgFe_2O_4$*	565	406	-	-
$ZnFe_2O_4$*	555	393	325	169
$CoFe_2O_4$*	575	374	320	181

* Literature Values.

of our samples. Hence ν_3 band can be assigned to the $Co^{2+} - O^{2-}$ octahedral complexes (Fig.4.6,4.7).

Josyulu and Sobhanadri[38] had noticed the same behaviour during their IR study on Co-Zn and Mg-Zn ferrites. Recently Badarinath[39] has observed ν_3 band around 370 cm^{-1} by introducing Al^{3+} into the lattice of $MgFe_2O_4$ and observed the increase in intensity with increasing concentration of Al^{3+}. Therefore it can be concluded that the appearance of ν_3 band in the spectra of present samples (Fig.4.6,4.7) is due to the divalent metal ion-oxygen complexes in the octahedral sites.

The method of preparation, grain size and porosity play an important role in locating the band positions. Hence the observed changes in the positions of band (Table 4.3, Fig.4.6 to 4.8) are attributed to above influencing factors.

The presence of Fe^{2+} ions causes the splitting of the absorption band due to local lattice deformations caused by Jahn-Teller effect in Fe^{2+} ions leading to the non-cubic component in the potential of crystal field. Whereas Fe^{3+} ions electronic configuration do not undergo Jahn-Teller distortion and hence no splitting is observed. In the present

case, one of the spectra is in good agreement of the above results. Such results were observed by Murthy and others[40] in the Mossbauer and infrared studies of some nickel-zinc ferrites.

In this way the present studies on IR spectra of $Cu_xCo_{1-x}Fe_2O_4$ reveal that the absorption spectra around 600 cm^{-1}, assigned to tetrahedral complexes, does not show any splitting and hence the possibility of Fe^{2+} ions at A site is ruled out. Whereas the splitting in the absorption band around 400 cm^{-1}, assigned to octahedral complexes, suggests the possibility of Fe^{2+} ions at B site. Morever the results are in general agreement with the literature values.

REFERENCES

1. Alper, A.M. in " High Temperature Oxides "
   Academic Press New York (N.Y), (1971).
2. Jain, G.C, Das, B.K, Khonduja, R.S. and Gupta, S.C.
   J. Mat. Sc. (GB) Vol.11, No.7, p-1335-38, (1976).
3. Neel, L. Ann. Phy. (Paris) 3, 137, (1948).
4. Weiss, P. J. Phy. Theo. Appl. 6, 667, (1907).
5. Gorter, E.W. and Schulkes, J.A. Phy.Rev.90, 487,(1953).
6. Smart, S. Amer. J. Phy. 23, 356, (1955).
7. Yafet, Y. and Kittel, C. Phy. Rev.87, 290, (1952).
8. Lotgering, F.K. Phillips Res. Rept. 11, 190, (1956).
9. Lyons, D.H. and Kaplan, T.A. Phy. Rev. 120, 1580, (1960).
10 Corliss, L. and Hastings, J. J.Appl. Phy.335,
   1138, (1962).
11 Enz, U. Appl. Phy. 325, 22, (1961).
12 Kramers, H.A. Physica. 1, 182, (1934).
13 Anderson, P.W. Phy. Rev. 79, 350, (1950).
14 Pukhav, I.K., Davido Vich, A.G. Ziuovik, M.A. Iud.
   Lab. (U.S.A.), Vol.40, No.4, p.511-13, April,(1974).
15 Besenicar, S.D. Hanzel, D.
   J. Phy. Colloq. (France), Vol.46, No.C-6,
   p-169-74, Sep, (1985).

16 Mun Cheol, Paek Ho Bin Im-Su II Pyan. Trans. Korean Institute, Electr. Eng. Vol.32, No.1, p-24-9,(1983).

17 Prince, E. Neutron Diffraction Results of Heat Treatment in Cobalt Ferrite. Phy. Rev.102, 674-76, (1956).

18 Sawatzky, G.A. Vander Woude, F. and Morrish, H.A. J. Appl. Phy. 39, 1204-1206, (1968).

19 Wijn, H.P.J. and Smit, J. in " Ferrites " p-157, John Wiley and Sons, NY, (1959).

20 Bertaut, E. J. Phy. Radium 12, 252, (1951).

21 Patil, S.A. in " Ph.D. Thesis " Shivaji University, Kolhapur, (India), p-171, (1980).

22 Craik, D.J. and Griffiths, P.M. Brit. J. Appl. Phy. 9, p-905, (1958).

23 Perduijn, D.J. and Peloschek, H.P. Proc. Brit. Ceram. Soc. No.10, 263-73, (1968).

24 Jong-Tae Baek SuII, Pyan. Ho Bin Im. J. Korean Phy. Soc. Vol.16 No.1, 97-104, (1983).

25 Rikukawa, H. I.E.E.E. Trans. Magn. (U.S.A.), Vol. MAG-18, No.6, p-1535-37, Nov, (1982).

26 Waldron, R.D. Phy. Rev. 99, 1727, (1955).

27 Hafner, V.S. Z. Fur. Krist. 115, 331, (1961).

28 Tarte, P. Spectr. Acta. 21, 313, (1965).

29 Preudhomme, J. Spectr. Acta. 26-A, 985, (1970).

30 White, W.B. and De Angelis, B.A.
Spectr. Acta. 23-A, 985, (1967).

31 Brabers, V.A. Phy. Status. Solidi. (Germany),
Vol.$\frac{33}{2}$, p-563, (1969).

32 Klerk, J., Brabers, V.A. Solid State Commun,
(USA), Vol.$\frac{14}{7}$, p-613, April, (1974).

33 Slmsa, Z., Roskovec, V., Novak, P.
Czech. J. Phy. 21-B, 1187, (1971).

34 Kainuma, S. (Japan), J. Appl. Phy. 15, 1079, (1976).

35 Nishikava, T. Okamoto, Y. and Enomota, S.
J. (Japan), Soc. Powder and Powder Metallurgy.
27, 56, (1980).

36 Tarte, P. and Preudhomme, J.
Spectrochim. Acta. 27-A, 961, (1971).

37 Botakova, V.R., Zevrey, N.D. and Romanov, V.P.
Phy. Status. Solidi. (a), 12, 623, (1972).

38 Josyulu, O.S. and Sobhanadri, J.

Phy. Stat. Sol. (a), 65, 479, (1981).

39 Badarinath, K.V.S. Phy. Status. Solidi.(a), (Germany),

Vol. 91, No.1, Pk-19-22, 16 Sept, (1985).

40 Murthy, V.R.K., Sankar, S.C., Reddy, K.V. and

Sobhanadri, J. Indian J. Pure and Appl.

Phy. Vol. 16/2, p-79, Feb, (1978).